JOURNAL OF PROPULSION AND POWER
Vol. 10, No. 6, Nov.–Dec. 1994

F/A-18 Inlet Calculations at 60-Deg Angle of Attack and 10-Deg Sideslip

S. D. Podleski*
NYMA, Inc., Brook Park, Ohio 44142

This article presents the results of numerical calculations on a 19.78% scale forebody/inlet model of the F/A-18 at a Mach number of 0.20, an angle of attack of 60 deg, and a sideslip angle of 10 deg. The main purpose of these calculations is to support an upcoming wind-tunnel test program in the prediction of engine inlet compressor face total pressure recovery and flow distortion. The CFD model includes the inlet and lip, and other aircraft components that are considered to be important to inlet performance, such as the ramp/splitter plate, the diverter and leading-edge extension (LEX) slot, and the deflected leading-edge flap. The CFD show complex flow patterns on the fuselage surfaces below the LEX, on the ramp/splitter plate, inlet lip, and inside the inlet. The CFD tends to underpredict total pressure recovery and overpredict the flow distortion at the inlet compressor face.

Introduction

THE High Alpha Technology Program (HATP)[1] utilizes a specially equipped F/A-18, the High Alpha Research Vehicle (HARV), in an effort to improve the maneuverability of high-performance military aircraft at low-subsonic-speed, high angle-of-attack conditions. One of the goals of HATP is to accurately predict the aerodynamics of aircraft operating at extreme attitudes. This program consists of the study of the effects of high angle of attack, yawed flight on the external aerodynamics including thrust vectoring control systems and vortex flow control, and the internal aerodynamics of the flow through the engine inlet ducts. The overall objective of the internal aerodynamics effort is to develop inlet technology that will ensure efficient airflow delivery to the engine during these maneuvers. One part of this effort utilizes CFD codes to predict the installed performance of inlets for these highly maneuverable aircraft.

This article will present the results of calculations with PARC3D, a Reynolds-averaged Navier-Stokes code, on the F/A-18 at an angle of attack of 60 deg, a sideslip angle of 10 deg, and a Mach number of 0.2, with emphasis on inlet performance parameters. Particular attention was made to determine the effect of the forebody, the lower fuselage/leading-edge extension (LEX) corner, the ramp/splitter plate, the cowl and lip, and the diverter and LEX slot on the flow through the inlet and at the compressor face.

This effort is a continuation and improvement of the work by Bruns and Smith,[2] who calculated the flow around symmetrical geometry of the F/A-18 at an angle of attack of 30 deg. These calculations were made in support of a proposed 19.78% scale-model wind-tunnel test program. Although data at comparable conditions are not available for the present case, the work by Bruns and Smith provides some confidence in the capture of the primary flow features.

The following discussion will begin with a short description of the PARC3D code, the grid geometry and flow boundary conditions. A detailed description of the external flow in proximity of the inlet and the flow through the inlet follows. This article then concludes with a short discussion of ongoing and future work.

Received May 7, 1993; presented as Paper 93-1806 at the AIAA/SAE/ASME/ASEE 29th Joint Propulsion Conference and Exhibit, Monterey, CA, June 28–30, 1993; revision received May 6, 1994; accepted for publication May 11, 1994.

*Senior Engineer, Propulsion Aerodynamics Section.

PARC3D Code

The PARC3D code[3] solves the full three-dimensional Reynolds-averaged Navier-Stokes equations in strong conservation form using the Beam and Warming approximate factorization scheme to obtain a block tridiagonal system of equations. The computational domain is decomposed into discrete blocks in which block matrix inversion takes place. PARC3D allows the use of multiple grid block, which simplifies the generation of grids around complex shapes. The Pulliam's scalar pentadiagonal transformation provides an efficient solver. The code uses a modified Baldwin-Lomax turbulence model that does not use the streamwise component of vorticity in the determination of the turbulence length scale.[4] This approach was found to improve the modeling of vortical flows in ducts. The use of the Baldwin-Lomax turbulence model, although developed for unseparated flow, was dictated by its availability within the code.

Geometry and Grid Definition

The grid geometry is based on the full-scale HARV F/A-18. Most of the significant geometry was modeled except for the empennage, most of the fuselage aft of the wing, ramp bleed, and two vortex generators located inside the inlet. The noteworthy components modeled are the inlet, ramp/splitter plate, diverter and LEX slot, inlet cowl, and leading-edge flap fully deflected at 34 deg. The grid was created using the GRIDGEN system[5] and is comprised of 30 blocks that total approximately 2.4 million grid points. Figure 1 shows the grid blocks structure. The overlapping block boundaries are required by the PARC3D code in order to pass interblock flow information. The flap grid overlaps the upper and lower wing grids; the inlet lip grid overlaps the inlet and cowl grids. The use of overlapping grids easily allows the addition of geometry elements and also allows better resolution of complex geometries with less effort on grid generation. Figure 2 illustrates the symmetry plane and surface grids of the half-model.

As an indication of grid density, the $y+$ values near the corner of the lower surfaces of the LEX and fuselage varied between 0.5–2.2; the $y+$ at the ramp/splitter plate varied between 0.1–1.3; the inlet values are between 1.6–2.6, whereas the values on the inlet lip are between 0.5–2. The grids on the upper surfaces are less densely packed and were modeled as Euler zones since it was assumed that these surfaces have

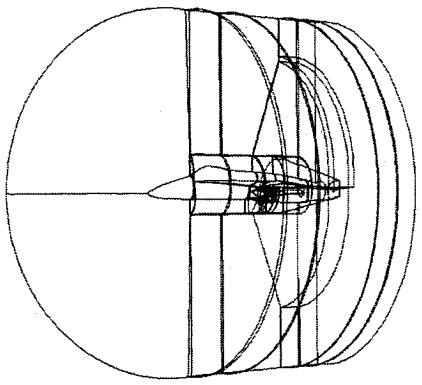

Fig. 1 Grid block structure.

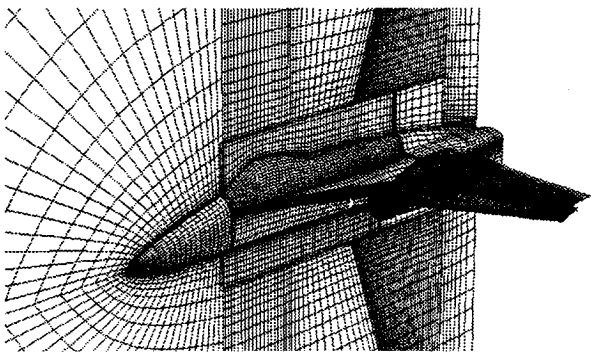

Fig. 2 Flowfield and surface grids.

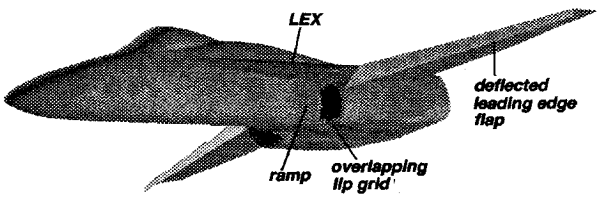

Fig. 3 Shaded wall geometry.

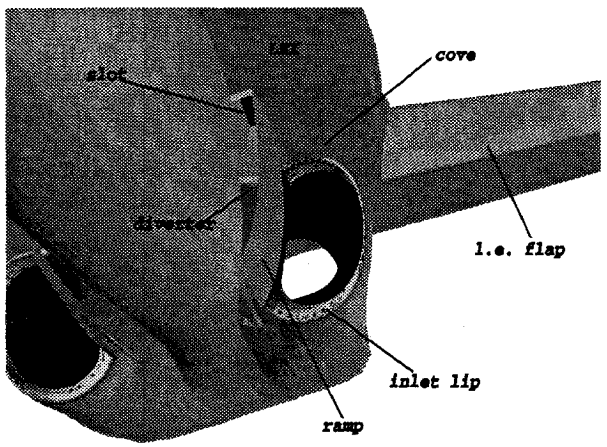

Fig. 4 Surface geometry near inlet.

negligible influence on the inlet flow although Murman et al.[6] state that CFD calculations have found that the inlet flow has a strong effect on the vortex above the LEX. Typical $y+$ values for the Euler regions are between 15–75 for the canopy and upper LEX surfaces. Although the flap and wingtip caps were not explicitly modeled, symmetric-plane boundary conditions were used by adjacent-block, neighboring grid points that do not have any boundary-condition data through interblock interpolations. Figure 3 is a shaded-wall diagram of the full model whose inlet region detail is shown by Fig. 4.

Boundary Conditions

Adiabatic, nonslip wall conditions were used on the forebody, the fuselage surface below the LEX, the LEX lower surface, the splitter plate/ramp, diverter and LEX slot, inlet, and the lower wing and flap surfaces. All other surfaces, including most of the leeward surfaces, were modeled with adiabatic slip condition. Trilinear interpolation was used to transfer data between blocks.

The outer boundaries assumed sea level, standard day, freestream conditions, at a Mach number of 0.2, an angle of attack of 60 deg, and sideslip angle of 10 deg with the wind off the aircraft's right side (as seen by the pilot). This type of condition uses the one-dimensional Riemann invariant to maintain freestream conditions. The compressor face was modeled as a static pressure surface whose magnitude was determined by the desired full-scale corrected mass flow of 144 lb/s. These freestream conditions and corrected mass flow result in a relatively high inlet capture ratio of 1.8.

Numerical Issues

External flow solution convergence was determined by monitoring the iteration history of lift and drag coefficients, while inlet mass flow axial variation, the iterative variations of the fan face total pressure recovery and distortion, were used to determine internal flow convergence. Axial mass flow, fan face total pressure recovery, and distortion variations near convergence were less than 2%; the variation of the lift and drag coefficients were less than 10%.

A total of 8000 iterations were completed, with one iteration taking 1 min of Cray Y-MP CPU time. The largest grid block occupied approximately 16 MWords of memory.

Results

A discussion will now be given of the PARC3D calculations. First will be a description of the portion of the external flow that has significant effect on inlet flow quality. The flow description will include plots of limiting streamlines and free particle traces. This will be followed by a discussion of the inlet internal flow with a presentation of inlet entry and compressor face axial vorticity and total pressure contour plots; comparisons are then made with available flight-test data.

External Flow

Figure 5 shows the particle traces as computed by the PLOT3D graphics program.[7] The flow features of note are the separated flow off the forebody and LEX, the vortices generated at the lower corner of the LEX and fuselage surfaces, and the flow coming off the flap. The vortical flow along the lower fuselage/LEX corner is different from that reported by Bruns and Smith,[2] where at an angle of attack of 30 deg, a single fuselage/LEX corner vortex was convected downstream and ingested by the inlet. In the present case, where the angle of attack is 60 deg, the flow along the lower fuselage/LEX corner has some of the characteristics of stag-

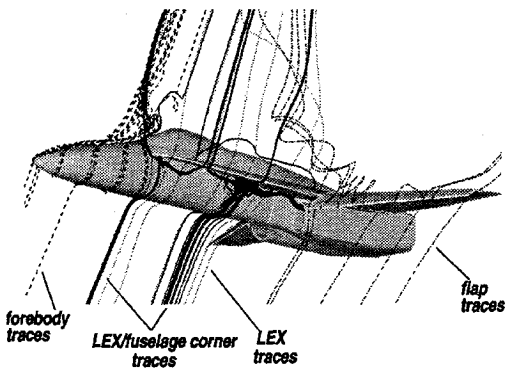

Fig. 5 Particle traces.

nation flow in that some of the flow moves upstream. The traces drawn as solid lines in Fig. 5 show the generation of vortex pairs near the lower fuselage/LEX corner. Although Fig. 5 shows two such pairs, one near the LEX apex and the other midway down the LEX, at least another pair, in the form of a horseshoe vortex, is located slightly upstream of the inlet. One vortex of each pair moves upstream while the other moves downstream. The vortex pair near the LEX apex shows the downstream-moving vortex colliding with an upstream-moving vortex from the second pair; the merged vortices move over the LEX leading edge into the aircraft wake. The downstream-moving vortex of the second-pair is relatively strong until it is split by the ramp/splitter plate; this weakened vortex is ingested by the inlet while the remainder is dumped overboard by the diverter, exiting through the LEX slot where it is engulfed by the wing's wake.

Figure 5 also shows particle traces over the forebody; the flow direction is from the leeward to the windward side with no flow aft, along the fuselage. The flow off the LEX, shown as lightly shaded dotted traces, is not the conventional slender-wing, leading-edge vortex, but is separated because of the high angle of attack. The flow over the flap, shown as dashed traces, moves towards the tip until the inboard flow is caught by the separated wing flow that forces it inboard. Because of the proximity of the inboard tip of the deflected flap, an initial concern was the inlet ingestion of the flap tip vortex. No flow off the inboard end of the deflected flaps is ingested by the inlet.

An important concern for engine performance is the ingestion of low energy, distorted flow generated by the aircraft components upstream of the inlet. The forebody and lower fuselage/LEX corner are possible sources of this low energy, distorted flow. Limiting streamlines or oil flow patterns may outline regions of separated flow. Limiting streamlines are also known as skin friction lines, and can be visualized in wind-tunnel and flight tests by releasing oil droplets on the surface of the test body. Figure 6 shows the PLOT3D-generated limiting streamlines flow patterns over the forebody. Because of the yawed flow, the separation and reattachment lines do not have a symmetrical pattern. No secondary cross-stream separation lines are seen as by Fisher et al.[8] This may be due to insufficient grid density as Smith and Podleski[9] indicate that increased grid density will capture secondary cross-stream separation. The flow patterns, shown by Figs. 5 and 6, indicate no flow off the forebody is ingested by the inlet. Figure 7a shows the limiting streamlines along the leeward fuselage below the LEX. A separation line is seen along the fuselage, originating from a saddle point below the LEX apex and extending to the splitter plate where the influence of the diverter bends the separation line upwards. Other separation lines branch into the main separation line. The ramp/splitter plate breaks the limiting streamline pattern on the fuselage and generates another separation line. A series of saddle points are located on the reattachment line along the LEX lower surface.

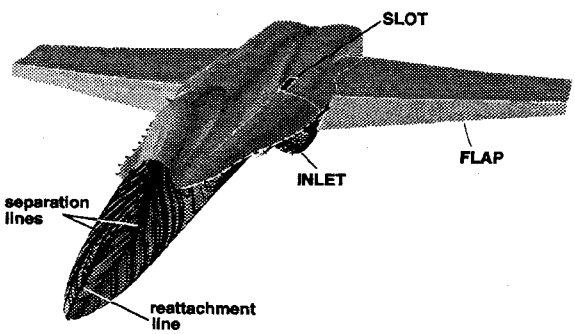

Fig. 6 Limiting streamlines along forebody.

The flow along the windward side shows no obvious separation lines along the fuselage except for a series of saddle points on the lower LEX and fuselage surfaces which are the origins of attachment or separation lines (Fig. 7b). The flow from the LEX lower surface moves downward along the fuselage. Similarly to the leeward side, a series of vortex pairs are located near the lower LEX/fuselage corner; these vortices are weaker and closer to the fuselage wall. Topology calculations by the FAST[10] graphics package show that the core of the vortex moving towards the inlet is ingested by the diverter.

Extremely small secondary crossflows exist at both LEX/fuselage corners, but the grid resolution may be insufficient or the sharp corner geometry may be unsuitable to give an acceptable solution.

The low Mach number and high inlet mass flow rate places the stagnation or attachment line on the cowl surface relatively far downstream of the inlet highlight. These conditions, in addition to the high angle of attack, cause a complex flow pattern in the upper diverter area between the lower LEX and upper cowl surfaces. In this area, the flow, including the low-energy boundary layer and separated flow off the cowl and LEX surfaces, moves upstream into the inlet; the contribution of this ingested low-energy flow to inlet performance could not be assessed. The study of the limiting streamlines will give an indication of the extent of this reverse flow. Figures 8a and 8b show the limiting streamlines along the leeward ramp/splitter plate, cowl, inlet, and upper diverter grid blocks; most of the other blocks were not drawn to avoid confusion. The limiting streamlines along the LEX lower surface (Fig.

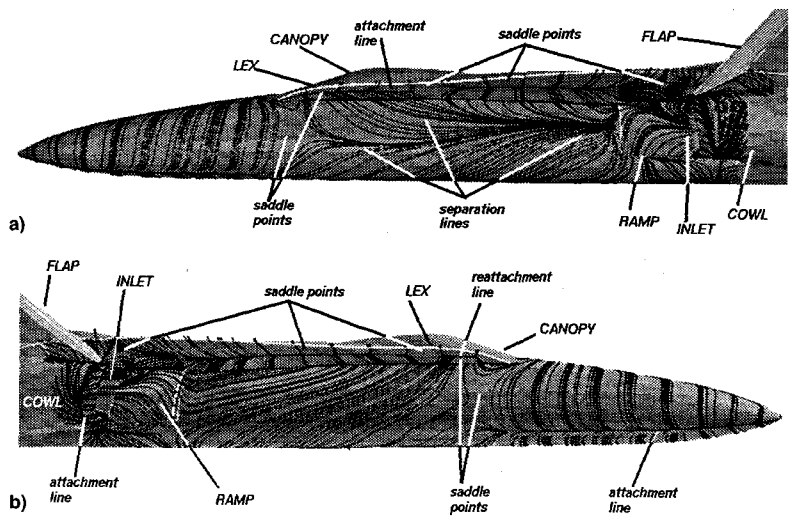

Fig. 7 Limiting streamlines along fuselage and LEX surfaces: a) leeward and b) windward.

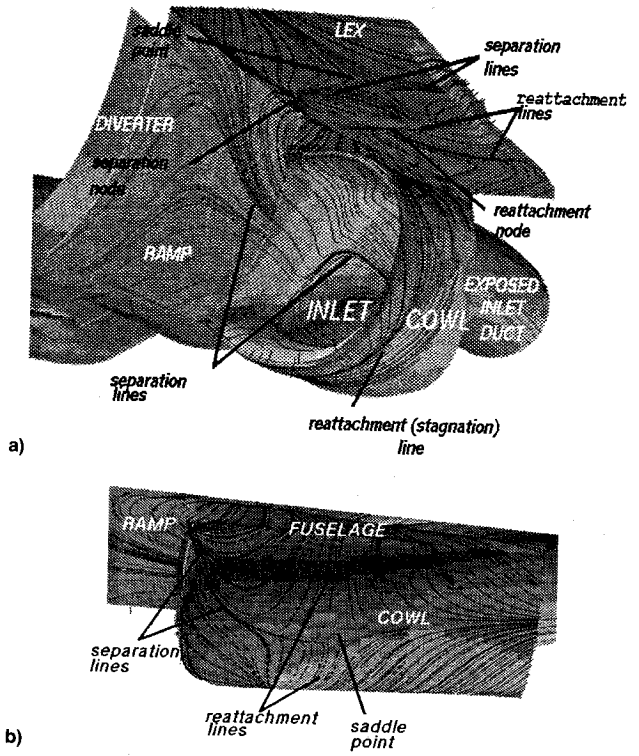

Fig. 8 Limiting streamlines along upper diverter surfaces: a) front and b) side view.

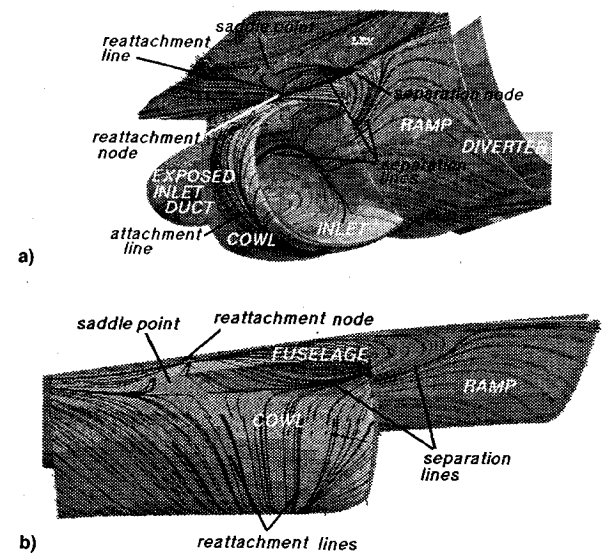

Fig. 9 Limiting streamlines on windward upper diverter surfaces: a) front and b) side view.

8a) show a saddle point of separation upstream of the inlet and a reattachment node downstream; these features provide a boundary of the reverse flow region. The inboard portion of a horseshoe vortex associated with the flow separation is ingested by the upper inboard corner of the inlet; the outboard portion of the horseshoe vortex is convected over the LEX leading edge. Figure 8b shows the limiting streamlines along the cowl where a saddle point of separation shows extent of the reverse flow on the cowl surface.

The windward upper diverter reverse flow (Figs. 9a and 9b) boundaries show a similar but smaller extent of reverse flow. The reattachment node, located on the LEX/fuselage corner, provides a downstream reverse-flow boundary through a reattachment line that lies approximately 45 deg across the lower LEX surface.

Internal Flow

The following will be a discussion of the flow inside the leeward and windward inlets with a description of the separated flow inside the lip and cross-sectional views of the axial component of vorticity and total pressure contours at the inlet entry and compressor faces.

Figure 10a shows the limiting streamlines inside the leeward lip and inlet. The flow separates along the lateral edge of the lip where the cross-sectional thickness is relatively thin, and along the bottom of the lip where the incoming flow angle is

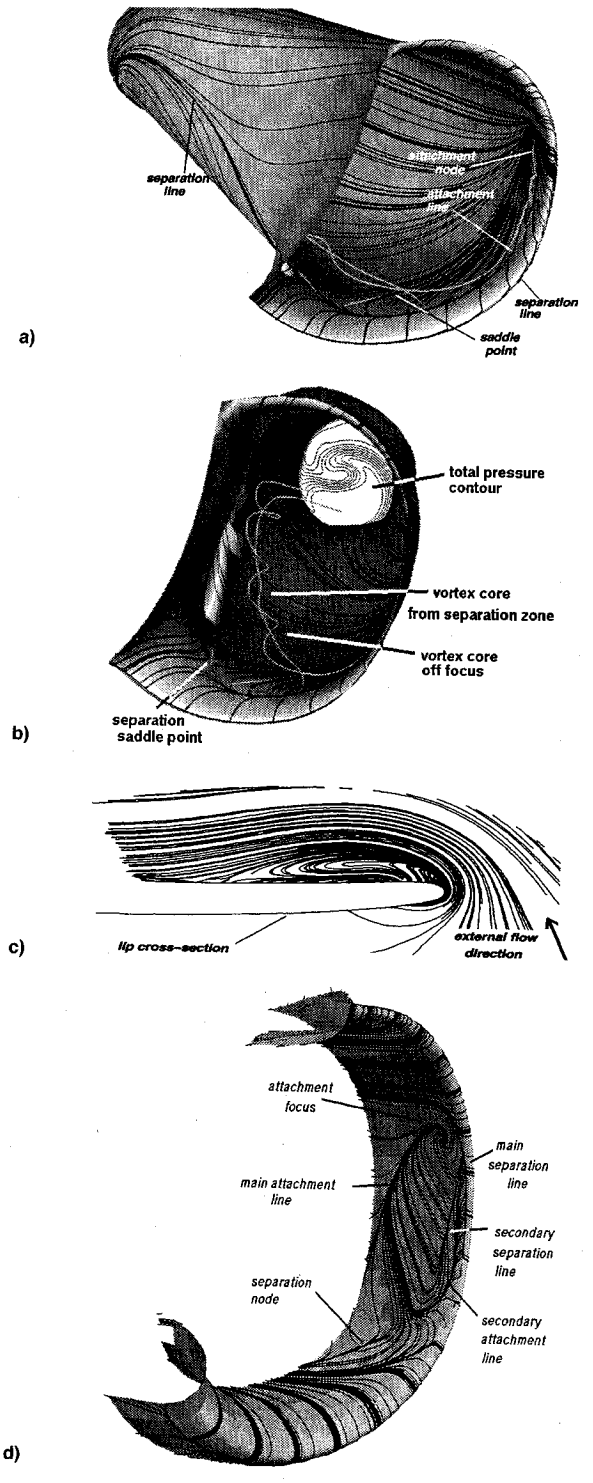

Fig. 10 a) Limiting streamlines inside leeward inlet and lip-3/4 view, b) limiting streamlines inside leeward inlet and lip-front view, c) cross-sectional view of separated flow around lateral edge of leeward inlet lip, and d) limiting streamlines on leeward lip at an angle of attack of 30 deg.

very high. Along the upper surface of the lip, where the cross-sectional thickness is larger and the flow turning angle is relatively small, the flow is unseparated. At this Mach number and mass flow rate, the stagnation or attachment line is on the outside wall of the lip with the separation line located just inside the highlight. Inside the lip, the limiting streamlines of a large separation zone is anchored at one end by a focus high on the lateral edge, and on the other end by a separation saddle near the low inboard corner. The FAST topology module found two major vortices inside the inlet; Figs. 10a and 10b show the traces of the vortex cores.

The main vortex originates in the separation zone, and is convected along the inboard bottom corner of the inlet. This vortex is responsible for the large region of low total pressure at the compressor face; more details of the low-pressure region will be given later. Another vortex lifts off the focus and travels down the separation zone until it joins the main vortex.

Figure 10c is a cross-sectional view of the particle traces around the lateral edge of the leeward inlet.

The resolution of the separated flow near the lip is somewhat diffuse because of the poor interblock communication of data from the high-grid density lip block to the lower-grid density inlet block. This deficiency was corrected in later work with a symmetric geometry of the F/A-18 at 30-deg angle of attack and no yaw angle.[11] Figure 10d shows the result of the improved interblock communication; a secondary separation zone is now visible.

The main vortex seen in Figs. 10a and 10b may be the result of the rollup of the separation sheet emanating from the separation saddle. Figure 11 shows the downstream evolution of the resultant cross-stream separated flow in the form of cross-sectional total pressure contours of the leeward inlet. As this cross-stream separated flow moves downstream into the inlet, it initially moves towards the inboard wall where it coalesces with the upper and lower corner flows and then moves outboard to its final position at the compressor face. This migration of the cross-stream flow can be better visualized with the use of the FAST graphics package that allows animation of flow data. A more detailed discussion of the effect of this cross-stream separation on inlet performance is given below.

Figure 12 is a comparison of the total pressure contours at the windward and leeward inlet entrance and compressor faces; the observer is upstream of the inlet and looking downstream. The low-pressure region on the leeward compressor face has an inverted comma shape that occupies the lower half of the compressor face. This low-pressure region is the result of the lip separation vortex mentioned above. Figure 12 also shows the total pressure of the leftside inlet with no sideslip. The

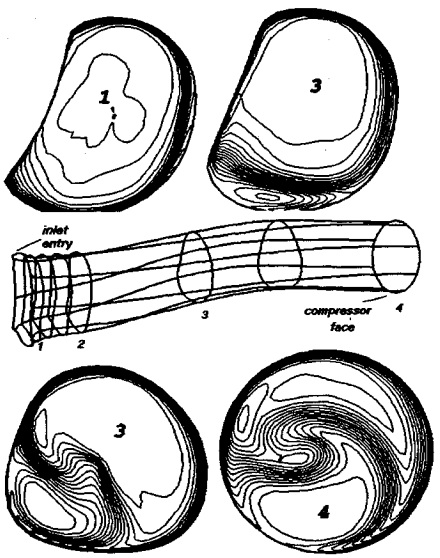

Fig. 11 Cross-sectional total pressure contours of leeward inlet.

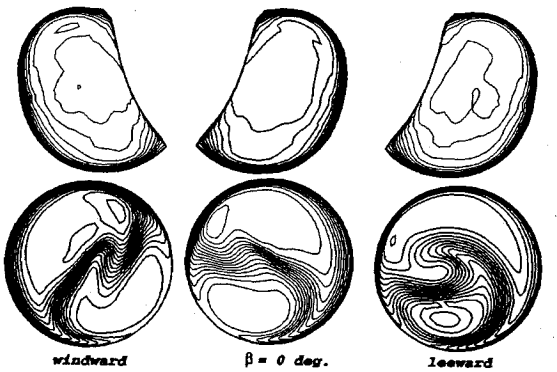

Fig. 12 Total pressure contours at inlet entry and compressor faces.

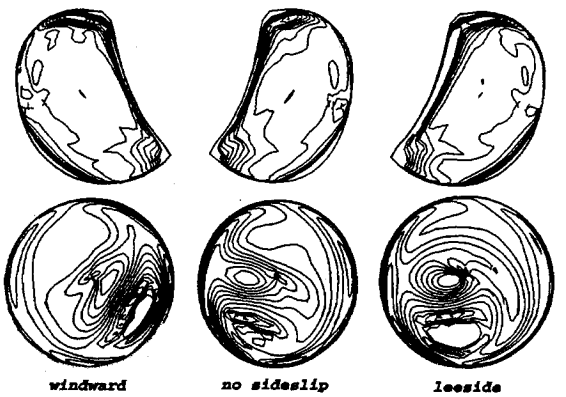

Fig. 13 Axial component of vorticity at inlet entry and compressor faces.

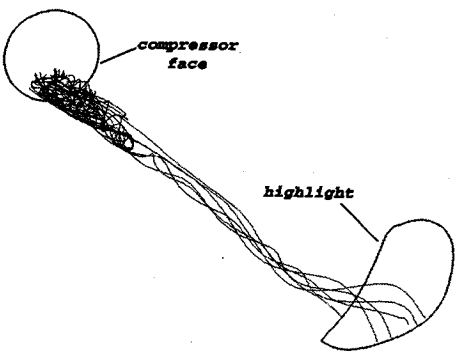

Fig. 14 Streamwise separation at leeward compressor face.

total pressure contours near the inlet entry indicate that the boundary layer at the bottom inboard corner of the inlet is thicker for the leeward inlet than for the windward inlet.

Figure 13 shows the axial vorticity contours at the inlet entry and compressor face. Another, but smaller, vortex is located near the center of the leeward compressor face. With the use of the particle trace option of PLOT3D, the origin of this vortex was found to be a combination of the ingested LEX/fuselage vortex and flow off the lower edge of the ramp; the limiting streamline traces on the ramp/splitter plate are shown by Figs. 7a and 8a. Although not seen in Fig. 13, a similar but much smaller vortex is located near the center of the windward compressor face. The vortex for the non-sideslip case is similar to that in the leeward inlet. The axial vorticity contours at the inlet entry show some cross-stream separation near the upper inboard corner of the inlet; this may be due to the ingestion of the horseshoe vortex mentioned previously. On the leeward compressor face, near the center of the low-pressure region is a region of reverse flow. Figure 14 shows particle traces that were seeded in this region. It shows a

sudden expansion of the crossflow. The validity of this reverse flow is uncertain because of the approximate nature of the downstream boundary condition that assumes a constant static pressure. The reverse flow in this area causes the code to switch from a static pressure to a total pressure boundary condition in the reverse flow region. A more realistic boundary condition simulating the effects of a fan may redistribute the low-pressure flow and prevent this streamwise flow separation. There is a similar, but smaller, region of streamwise flow separation in the windward inlet.

The reduction of the numerical results at the compressor face follows that of Northrop wind tunnel[12] and flight tests.[13,14] In these tests, a rake, with eight equally-spaced legs, was positioned ahead of the compressor face station. Each leg had five steady-state and dynamic total pressure sensor pairs whose placement was based on equal area coverage. The steady-state probes have a low-frequency response and, therefore, are an indication of the time-averaged total pressure. The CFD data, corresponding to the sensor positions, were used to calculate total pressure recovery and flow distortion. Figure 15 shows the rake used to calculate CFD-based performance data; the rake is slightly distorted since the nearest grid point was used in these calculations. Figure 15 also shows the actual grid used by PARC3D to calculate the compressor face flow solution.

As was mentioned previously, the CFD calculations were done in support of proposed wind-tunnel tests that predetermined Mach number and model scale. The scale of the model was determined by the availability of a 5.5-in. fan simulator, and the choice of Mach number was limited by the maximum Mach number attainable by the NASA Lewis Research Center 9 × 15 wind tunnel. Since the wind-tunnel tests are to be undertaken in the future, some comparisons with existing data was needed to measure the capability of the code. The flight tests[12,13] were not conducted at the same conditions as used by the CFD calculations. The most similar conditions found were at a Mach number of 0.27, angle of attack of 61 deg, and yaw angle of 12 deg for the windward inlet, and a Mach number of 0.26 deg, angle of attack of 56 deg, and yaw angle of 8.4 deg. Different conditions existed for both inlets because only the left-side engine was instrumented and the aircraft flew at negative and positive yaw angles in order to obtain yaw effects. Positive yaw angle is defined with the velocity vector on the right side of the aircraft. The test data were measured by steady-state and dynamic instrumentation; the dynamic total pressure plots were given at peak fan sensitivity as defined in Vol. 1 of Ref. 12. Both sets of data are compared with the CFD, even though the PARC3D solutions are asymptotically steady state. This was done since wind-tunnel[14] and flight tests[12,13] show that flow through the inlet seems to have a significant unsteady component. Figures 16a and 16b show the percentage deviation of the total pressure from the average total pressure compared to flight tests; each contour represents a 2% increment. The observer is located downstream of the compressor face and looking upstream, therefore, the point of view is reversed from previous figures. Calculations show a low-pressure knot that is also shown by the dynamic distortion at peak fan sensitivity test results; the steady-state instrumentation tends to average out any unsteadiness that is present.

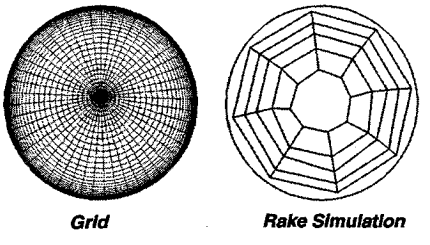

Fig. 15 Comparison of grid and rake grid density.

Table 1 Comparison of PARC3D and flight-test performance data

	PARC3D $\beta = 0$	PARC3D (no flap)	PARC3D (flap)	Flight data
	Windward inlet			
Recovery	88.6	88.8	87.2	92.0
Distortion	34%	31%	37%	24%
Fan face Mach no.	0.47	0.46	0.47	N/A
Corrected flow	5.66	5.68	5.57	5.59
	Leeward inlet			
Recovery	88.6	87.7	86.4	93
Distortion	34%	32%	36%	30%
Fan face Mach no.	0.47	0.45	0.46	N/A
Corrected flow	5.66	5.59	5.53	5.63

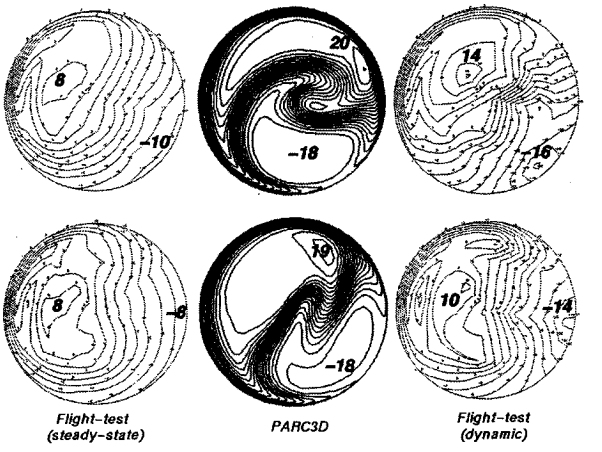

Fig. 16 Inlet compressor face normalized total pressure: a) leeward and b) windward.

Table 1 compares the inlet compressor face performance. The flow distortion measure used is the difference between the maximum and minimum total pressure normalized by the average total pressure. The use of this measure is a severe test of the CFD code, as many other measures of flow distortion are integral or averaging quantities. The distortion of the leeward inlet is about 1% lower than that of the windward inlet, and the pressure recovery is approximately 1% lower. Table 1 also shows the results for the case of no sideslip where the pressure recovery is higher and flow distortion is lower. This does not agree with test results[12,13] that show that the no-sideslip case has pressure recovery in between the leeward and windward inlets. Table 1 further shows that a deflected flap sightly decreases pressure recovery and significantly increases flow distortion as compared with the no-flap case. This may be due to the beneficial effect of the flap on wing lift, which in turn would increase the induced angle of the flow entering the inlet.

Comparison with flight-test data shows that PARC3D underpredicts pressure recovery and overpredicts flow distortion. A partial explanation of this discrepancy is that the flight test was at a 30% higher Mach number which, as shown by more recent calculations with PARC3D, would reduce losses. Other causes may be due to insufficient axial and circumferential grid density, exclusion of the inlet vortex generator pair, and of course, a common culprit, if all else fails, may be the inadequacy or unsuitability of the turbulence model.

Conclusions and Future Work

PARC3D calculations on the F/A-18 at an angle of attack of 60-deg sideslip of 10 deg and Mach number of 0.20, compare favorably with flight-test data. A complex pattern of limiting streamlines on the lower LEX and fuselage surfaces indicate an external flow significantly different from that of

lower angles of attack. Flow distortion at the compressor face is considerably higher and total pressure recovery is significantly lower. PARC3D tends to underpredict compressor face pressure recovery and overpredict compressor face flow distortion.

Future work will increase the grid density of the lip to better resolve the complex entry flow, and include the two vortex generators located inside the inlet. Other improvements under consideration include the addition of increasingly realistic compressor face boundary conditions such as the fan simulator and the use of time-accurate algorithms in the PARC3D code. Various turbulence models are being tested in other applications and may be used in future PARC3D calculations of the F/A-18.

The complexity of the exterior flow in proximity of the inlet and internal flow through the inlet hindered a thorough comprehension of the implications of the CFD calculations; the source and degree of contribution to compressor face flow distortion by various aircraft components and flow features are not clearly understood and may require a more fundamental study.

Acknowledgments

Support of this work by the NASA Lewis Research Center of the National Aeronautics and Space Administration and under Contract NAS3-25266 is gratefully acknowledged. The interest shown by Project manager, Richard R. Burley, is particularly appreciated.

References

[1]Burley, R. R., Anderson, B. H., Smith, C. F., and Harloff, G. J., "High Alpha Inlets," Aeropropulsion '91, LeRC, NASA CP 10063, Cleveland, OH, March 1991.

[2]Bruns, J. E., and Smith, C. F., "Full Navier-Stokes Calculations on the Installed F/A-18 Inlet at a High Angle-of-Attack," AIAA/SAE/ASME/ASEE 28th Joint Propulsion Conf. and Exhibit, Nashville, TN, July 1992.

[3]Cooper, G. K., and Sirbaugh, J., "The PARC Distinction: A Practical Flow Solver," AIAA Paper 90-2002, July 1990.

[4]Sirbaugh, J. R., and Reichart, B. A., "Computation of a Circular-to-Rectangular Transition Duct Flow Field," AIAA Paper 91-1741, June 1991.

[5]Steinbrenner, J. P., Chawner, J. R., and Fouts, C. L., "The Gridgen 3D Multiple Block Grid Generation System. Vol. II: User's Manual," WRDC-TR-90-3022 Vol. II, Wright-Patterson AFB, OH, July 1990.

[6]Murman, S. M., Rizk, Y. M., and Schiff, L. B., "Coupled Numerical Simulation of the External Engine Inlet Flows for the F-18 at Large Incidence," AIAA Paper 92-2621, June 1992.

[7]Walatka, P. M., Buning, P. G., Pierce, L., and Elson, P., "PLOT3D User's Manual," NASA TM 101067, July 1992.

[8]Fisher, D. F., Banks, D. W., and Richwine, D. M., "F18 High Alpha Research Vehicle Surface Pressures: Initial In-Flight Results and Correlation with Flow Visualization and Wind-Tunnel Data," NASA TM 101724, 1990.

[9]Smith, C. F., and Podleski, S. D., "Thin Layer and Full Navier-Stokes Calculations for Turbulent Supersonic Flow over a Cone at an Angle-of-Attack," NASA CR 189103, Nov. 1993.

[10]Walatka, P. M., Clucas, J. C., McCabe, R. K., and Plessel, T., "FAST User Guide," NASA Ames Research Center, RND-93-01U, Moffett Field, CA, June 1993.

[11]Smith, C. F., and Podleski, S. D., "Installed F/A-18 Inlet Flow Calculations at 30° Angle-of-Attack: A Comparative Study," NASA CR 195297, April 1994.

[12]Amin, N. F., Richards, C. J., De La Vega, E. G., and Dhanidina, M. A., "F/A-18A Engine Inlet Survey Report. Vols. 1, 2, and 3," Northrop Corp, Aircraft Div., NOR 81-316, Hawthorne, CA, May 1977, Nov. 1981.

[13]Amin, N. F., and Hollwenger, D. J., "F/A-18 Inlet/Engine Compatibility Flight Test Results," *Journal of Aircraft*, Vol. 20, No. 8, 1983, pp. 641–649.

[14]Amin, N. F., Franks, W. J., De La Vega, E. G., Yamada, M., Hollweger, D. J., and Tsukahira, T. W., "AEDC Series 1 F-18 .192 Scale Inlet Test Analysis Report. Vols. 1, 2, and 3," Northrop Corp, Aircraft Div., NOR 77-310, Hawthorne, CA, May 1977.